

MMGT: Motion Mask Guided Two-Stage Network for Co-Speech Gesture Video Generation

Siyuan Wang*, Jiawei Liu*, *Member, IEEE*, Wei Wang[†], Yeying Jin, *Member, IEEE*,
Jinsong Du, Zhi Han, *Member, IEEE*

Abstract—Co-Speech Gesture Video Generation aims to generate vivid speech videos from audio-driven still images, which is challenging due to the diversity of different parts of the body in terms of amplitude of motion, audio relevance, and detailed features. Relying solely on audio as the control signal often fails to capture large gesture movements in video, leading to more pronounced artifacts and distortions. Existing approaches typically address this issue by introducing additional a priori information, but this can limit the practical application of the task. Specifically, we propose a Motion Mask-Guided Two-Stage Network (MMGT) that uses audio, as well as motion masks and motion features generated from the audio signal to jointly drive the generation of synchronized speech gesture videos. In the first stage, the Spatial Mask-Guided Audio Pose Generation (SMGA) Network generates high-quality pose videos and motion masks from audio, effectively capturing large movements in key regions such as the face and gestures. In the second stage, we integrate the Motion Masked Hierarchical Audio Attention (MM-HAA) into the Stabilized Diffusion Video Generation model, overcoming limitations in fine-grained motion generation and region-specific detail control found in traditional methods. This guarantees high-quality, detailed upper-body video generation with accurate texture and motion details. Evaluations show improved video quality, lip-sync, and gesture. The model and code are available at (<https://github.com/SIA-IDE/MMGT>).

Index Terms—Spatial Mask Guided Audio Pose Generation Network (SMGA), Unified model, Motion-masked hierarchical audio attention (MM-HAA)

I. INTRODUCTION

CO-SPEECH face and gestures, as typical non-verbal behaviors, play an extremely important role in human-human communication [4], [5]. In a speech video, the combination of the speaker’s head movements and gestures can

This work supported in part by National Natural Science Foundation of China under Grant U23A20343; Liaoning Provincial “Selecting the Best Candidates by Opening Competition Mechanism” Science and Technology Program under Grant 2023JH1/10400045

Siyuan Wang are with Shenyang Institute of Automation, Chinese Academy of Sciences, Shenyang 110016, P. R. China, Liaoning Liaohe Laboratory, the Key Laboratory on Intelligent Detection and Equipment Technology, Shenyang 110169, P. R. China, and also with the University of Chinese Academy of Sciences, Beijing 100049, P. R. China (e-mail: wangsiyuan@sia.cn).

Jiawei Liu, Wei Wang, and Jinsong Du are with Shenyang Institute of Automation, Chinese Academy of Sciences, Shenyang 110016, P. R. China, Liaoning Liaohe Laboratory, the Key Laboratory on Intelligent Detection and Equipment Technology, Shenyang 110169, P. R. China (e-mail: liujiawei@sia.cn; wangwei2@sia.cn; jsdu@sia.cn).

Yeying Jin was with the Tencent (e-mail: yeyingjin@global.tencent.com).

Zhi Han was with the State Key Laboratory of Robotics, Shenyang Institute of Automation, Chinese Academy of Sciences, Shenyang 110016, P. R. China (e-mail: hanzhi@sia.cn).

*These authors contributed equally to this work.

[†]Corresponding author: Wei Wang (email: wangwei2@sia.cn).

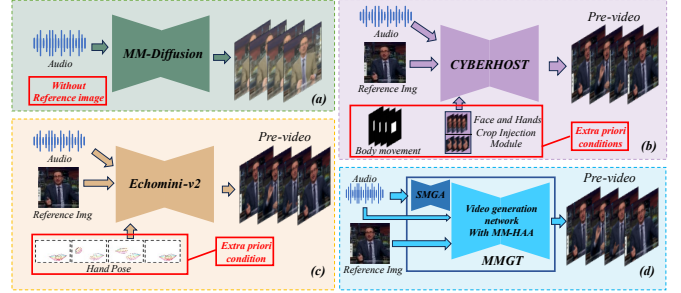


Fig. 1: Overview of existing models for generating videos of co-speech gestures. Compared with other methods [1]–[3], our method can generate videos of co-speech gestures for specified characters, and the generation for specific regions does not require additional prior information.

make a person’s speech more vivid and convey the meaning more clearly. Therefore, generating videos of the speaker’s gestures and head movements that are synchronized with the speech has attracted much attention from researchers. Unified audio-driven gesture and facial video generation has great potential for virtual worlds, Digital Human Development [6], and Multimedia Applications [7]. Although some current methods [1]–[3], [8]–[11] can generate vivid speech gesture videos, unfortunately, videos generated solely using audio and static images often suffer from low quality [8], [11]. On the other hand, some methods [1], [3] achieve better quality but introduce additional a priori information beyond audio and inferred images. These a priori elements are not as easily accessible as audio, which limits the practical application of the technology.

Existing methods mainly adopt end-to-end video generation frameworks. As shown in Fig. 1(a), MM-Diffusion [2] generates the full video directly from the audio based on a diffusion model, but does not introduce a reference image, resulting in an inability to effectively control the ID information of the characters in the video [11]. DiffTed [8] have used audio multi-stage to generate gesture videos, and EchoMimicV2 [1], CyberHost [3] have generated gesture videos by combining the audio with a priori information about the hand pose video or by utilizing codebook a priori enhancement techniques to generate gesture and face upper body videos. However, these methods still have several shortcomings. First, it is difficult to accurately control the synchronization of face and smooth movements of gestures simultaneously using only audio as a condition [2]. Second, most of the methods rely

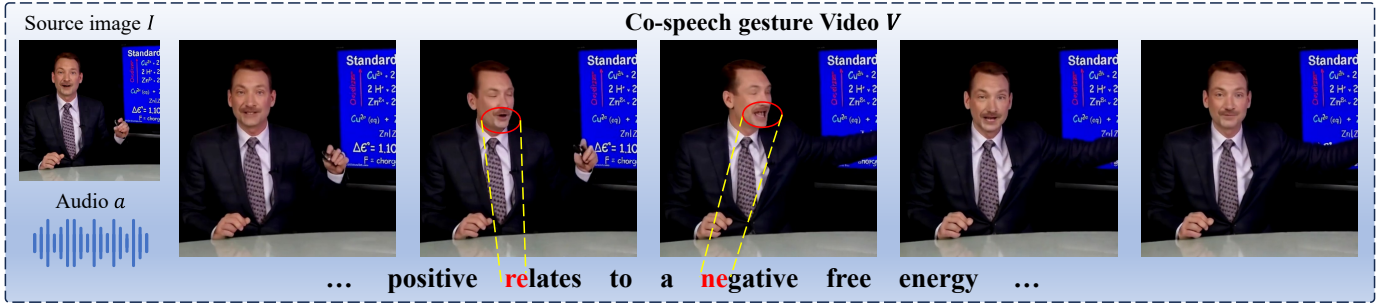


Fig. 2: Examples of our generated co-speech gestures video. The lips marked with red circles correspond to the bold red letters.

on other high-quality a priori conditions in addition to audio in the inference phase (see Fig. 1(b)(c)), which is limited in practical applications. Third, if the model lacks region-specific constraints, as show in Fig. 1(a), the generated video tends to have large deformations and distortions in critical regions (e.g., face, gestures). For example, when there are large movements such as head rotations, the generated video may show head distortion [8].

To address these challenges, we propose Motion Mask Guided Two-Stage Network (MMGT), which consists of two stages for video generation. In the first stage, we introduce the Spatial Mask Guided Audio Pose Generation Network (SMGA) to generate pose video guided by audio input. This pose video not only captures synchronized face but also naturally incorporates hand gestures. Based on this, as show in Algorithm 1, we further compute the maximum bounding box of each region to obtain motion mask.

In the second stage, we propose a novel Motion Masked Hierarchical Audio Attention (MM-HAA) Module, which leverages audio to dynamically enhance the details of specific semantic regions while pose sequences drive the motion of static images. By introducing this module, our framework can more accurately control the generation of simultaneous interpretation videos, as show in Fig. 2, significantly improving both realism and expressive fidelity.

As shown in Fig. 1, comparison of input requirements and output capabilities across different methods. Unlike EchoMimicV2 [1] and CyberHost [3], which require additional inputs such as hand pose sequences or body movement modules, our proposed method, MMGT, achieves synchronized generation of gestures and lip movements using only audio and a single reference image as inputs, without relying on any extra information. In summary, the main contributions of this work are as follows:

1. We propose the Spatial Mask Guided Audio Pose Generation Network to generate a pose video and a motion mask from a speech signal and an initial pose. This unified design ensures natural and synchronized control of face and hand movements, resulting in cohesive and realistic co-speech animations.
2. We introduce the Motion Masked Hierarchical Audio Attention Module for video generation. By integrating audio conditions with motion motion masks, the model adaptively focuses on specific semantic regions, such as hands, lips, and

face, enabling fine-grained detail enhancement.

3. Our network requires only audio and a single reference image as input to generate high-quality facial expression and gesture videos, without the need for additional prior information, significantly improving both practicality.

Extensive experiments demonstrate that our framework significantly outperforms existing methods in generating vivid, realistic, speech-synchronized, and temporally stable gesture videos. By effectively capturing the fine-grained synchronization of face and gestures with speech, MMGT advances the state-of-the-art in co-speech video generation, delivering results that are qualitatively and quantitatively superior to existing techniques.

II. RELATED WORK

A. Speech-driven Talking Face Video Generation

In the field of speech-driven talking face video generation, early studies primarily focused on the lip region, given its strong correlation with audio [12]. These works leveraged GAN-based networks [13] to synchronize lip movements in the video with the corresponding audio [14]. Subsequently, researchers extended audio-lip synchronization to achieve synchronized generation of audio-driven head movements, face and emotions [15]–[18]. Some studies leveraged pre-trained SD-diffusion models [19] to generate high-resolution and dynamic talking head videos from static images driven by audio [16], [20]–[22]. However, due to the limitations of existing models, it is challenging to extend face-specific video generation tasks to full upper-body video generation simply by retraining with a different dataset. Furthermore, current datasets also have inherent limitations: LRS2, VoxCeleb, and MEAD [23]–[25] only cover facial regions without including the full body, while the HDTF dataset [26] includes the entire upper body but lacks significant audio-correlated dynamic gestures. These issues collectively make it difficult for existing audio-driven talking face video generation methods to be adapted for gesture region synthesis. In contrast, our approach carefully considers the distinct correlations between facial and hand movements. By designing a well-structured network and utilizing the PATS dataset [27]–[29], our method effectively extends facial video generation to audio-driven upper-body video generation.

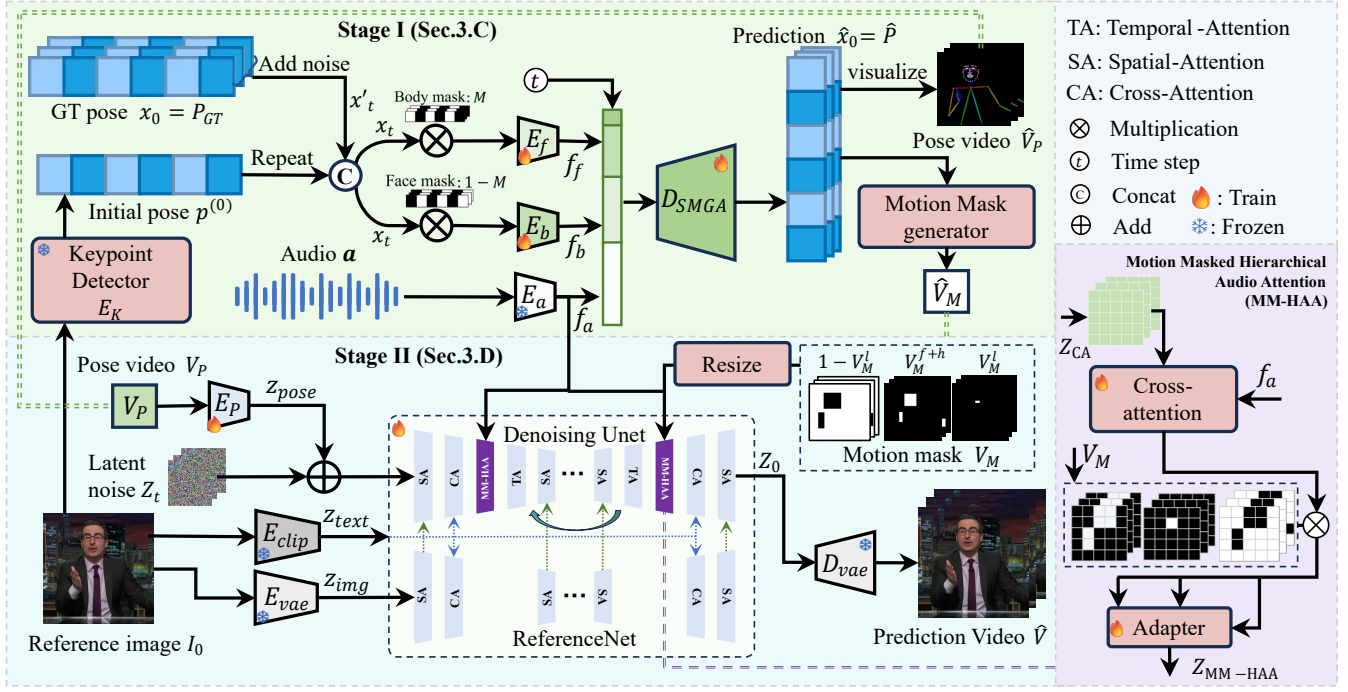


Fig. 3: Overview of the Proposed MMGT Framework. The framework operates in two stages: In Stage I, the SMGA network generates motion feature videos, including the pose video \hat{V}_P and motion mask \hat{V}_M , based on the input audio a and initial pose $p^{(0)}$. In Stage II, the Denoising UNet utilizes Z_{pose} and Z_{text} , while the ReferenceNet integrates Z_{pose} , Z_{text} , and Z_{img} to produce the final predicted video \hat{V} . On the right, the MM-HAA module enhances \hat{V}_M by aligning audio features f_a with cross-attention embeddings Z_{CA} . The green double dashed line indicates the inference process, where V_P and V_M are replaced by \hat{V}_P and \hat{V}_M when transitioning from training to inference.

B. Speech-driven Talking Gesture Generation

In the field of gesture generation, early studies primarily relied on human skeleton data to generate vivid gesture sequences driven by audio [30]–[32]. Recent research has incorporated multiple modalities based on audio, such as emotion [33] and style [32], to improve the controllability of gesture sequence generation. Methods like EMAGE [34] and DiffSHEG [35] have extended co-speech gesture generation to include head movement synthesis. However, these approaches often disregard appearance information entirely [11], resulting in outputs that fail to align with users’ visual perception.

C. Speech-driven Talking Gesture Video Generation

Currently, gesture video generation methods can be broadly categorized into retrieval-based and generation-based methods. Zhou et al. [36] were the first to frame gesture video generation as a task of reproducing video frames aligned with audio, achieving high-quality gesture videos through a video frame retrieval method. TANGO [9] further advanced this approach by employing an action graph-based retrieval technique to generate co-speech body gesture videos. While retrieval-based methods produce satisfactory results with limited computational resources, they face notable limitations, including the inability to synthesize novel gestures and the lack of correlation modeling between the speaker’s face and audio.

ANGIE [10] was the first to clearly define the problem of audio-driven gesture video generation, using unsupervised

features MRAA [37] to simulate body movements. However, due to the linear nature of MRAA, it cannot represent complex regions, limiting the quality of video generation. Additionally, methods such as [8], [11] use non-linear TPS transformation [38] to decouple human ANGIE [10] was the first to explicitly define the task of audio-driven gesture video generation, leveraging the unsupervised MRAA framework [37] to simulate body movements. However, due to its linear nature, MRAA struggles to capture complex motion regions, thereby limiting the quality of generated videos. More recent methods, such as [8], [11], adopt non-linear TPS transformations [38] to decouple human motion keypoints from images. These methods generate full keypoint sequences driven by audio, which are then used to produce compact optical flow for animating images and creating smooth gesture videos. Despite their advancements, generation-based approaches face common challenges: they fail to simultaneously generate detailed finger and lip movements, exhibit significant artifacts and deformation, and suffer from limited generalizability.

Our method introduces the Spatial Mask Guided Audio Pose Generation Network (SMGA) network, meticulously designed to implicitly generate keypoint sequences from audio. By integrating a multimodal video generation framework enhanced with the Motion Masked Hierarchical Audio Attention (MM-HAA) mechanism, the proposed approach drives a single static image to simultaneously produce dynamic co-speech gestures and talking head videos. Beyond generating speech videos

solely from audio, our method also supports pose-driven generation and joint driving with both pose and audio, providing greater flexibility and precise control over the output.

III. PROPOSED METHOD

We propose the **MMGT** network, as illustrated in Fig. 3, which ensures the synchronized control of both facial and hand movements, while also compensating for regional details. Given a segment of audio, we denote it as $\mathbf{a} = [a_0, \dots, a_N]$ and a reference image $I_0 \in \mathbb{R}^{3 \times W \times H}$, our framework generates a co-speech video consisting of N frames, denoted as $\hat{V} = [I_0, \hat{I}_1, \dots, \hat{I}_{N-1}] \in \mathbb{R}^{N \times 3 \times W \times H}$. The co-speech video generation process is divided into two stages, motion feature generation (Stage I), motion-driven and detail refinement (Stage II). Therefore, our inference pipeline can be formulated as

$$\hat{V}_P, \hat{V}_M = SMGA(E_k(I_0), a), \quad (1)$$

$$\hat{V} = \mathcal{G}_v(I_0, \hat{V}_P, \hat{V}_M, a). \quad (2)$$

where $E_k(\cdot)$ represents the initial pose extractor, responsible for obtaining the initial pose $p^{(0)}$ from the reference image I_0 . In the first stage, our proposed $SMGA(\cdot)$ network, built upon the DiT architecture [39], takes the audio a as a conditioning signal to generate the complete pose sequence \hat{x}_0 . In the second stage, the video generation model $\mathcal{G}_v(\cdot)$ incorporates an reference-net and a temporal module based on the SD architecture [40]. It leverages the motion mask \hat{V}_M generated in the first stage, along with the pose video and audio, as conditioning inputs to synthesize the final video \hat{V} .

A. Overall Framework Architecture

In the first stage, the SMGA network aims to capture the temporal and semantic relationships between motion features and audio input. As shown in Fig. 4, it consists of several key components. The motion block captures the correlation between audio and posture to obtain facial and overall posture features, and the merge block combines the two to obtain the final result.

In the second stage, the video generation network refines motion details using the generated motion features (motion mask, and pose videos), audio, and spatial cues from a reference image. This is achieved through a Denoising UNet, along with hierarchical attention module: Spatial Attention (SA) for texture details, Temporal Attention (TA) module for smooth transitions, and Motion Masked Hierarchical Audio Attention (MM-HAA) module for aligning audio with motion masks, ensuring temporal and spatial consistency in the generated video.

B. Motion feature generation

As illustrated in Fig. 3, the primary objective of the initial phase is to synthesize pose videos and motion masks using audio inputs as the driving force. To achieve this, we have developed a Spatial Mask-Guided Audio Pose Generation (SMGA) Network, which generates both the complete pose video \hat{V}_P and the corresponding motion mask \hat{V}_M . Among

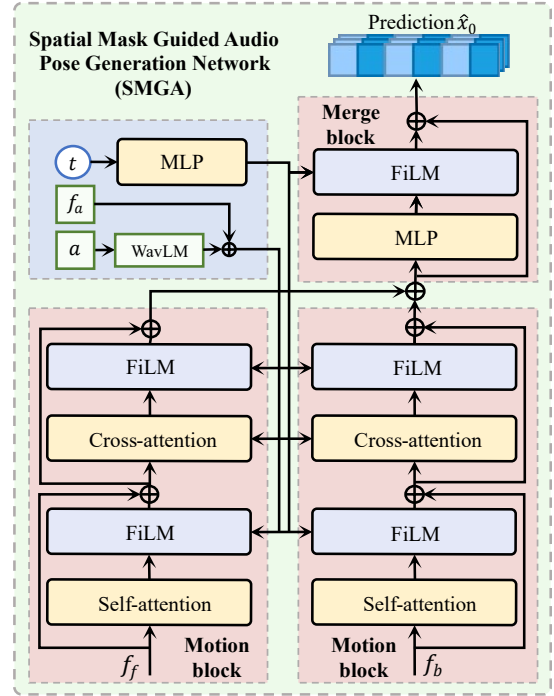


Fig. 4: Architecture of the SMGA network.

them, the pose video \hat{V}_P effectively captures the basic dynamics of the motion. The motion mask \hat{V}_M highlights key parts of significant motion, such as hands and faces, thus improving the accuracy of motion representation.

Conditional Input Preparation. The initial pose $p^{(0)}$ is extracted from the reference image I_0 using a pre-trained keypoint detector [41] E_K ,

$$p^{(0)} = E_K(I_0), \quad (3)$$

where $p^{(0)}$ represents the static pose keypoints of the subject in the reference image I_0 . To introduce variations for motion modeling, Gaussian noise is added to the ground-truth pose sequence P_{GT} to obtain noisy motion representations,

$$x'_t = P_{GT} + \mathcal{N}(0, \sigma^2), \quad (4)$$

where x'_t represents the noisy pose at time step t . The initial pose $p^{(0)}$ is repeated along the temporal dimension and added to x_t ,

$$x_t = x'_t + \mathcal{R}(p^{(0)}). \quad (5)$$

where $\mathcal{R}(\cdot)$ denotes the delayed time dimension replication N copies. Motion features have been categorized into facial expression motion features and gesture motion features as

$$x_t = [p^1, p^2, \dots, p^N] \in \mathbb{R}^{N \times (C_f + C_b) \times 3}, \quad (6)$$

where C_f corresponds to the keypoints relevant to head motion, while C_b corresponds to the keypoints for gesture

motion. To apply masking to x_t along the feature dimension C , we construct the mask M^f as

$$M^f = \begin{cases} 1, & \text{if } C \in C_f, \\ 0, & \text{otherwise.} \end{cases} \quad (7)$$

Next, the complementary mask M^b is obtained as $M^b = 1 - M^f$. These masks are then applied to the input x_t to isolate the respective feature representations, as defined below

$$x_t^f = x_t \odot M^f, \quad x_t^b = x_t \odot M^b, \quad (8)$$

where x_t^f and x_t^b correspond to the features for head and gesture pose sequence, respectively. Distinct encoders are employed to process these input conditions, transforming them into separate feature embeddings

$$\begin{cases} f_a = E_a(\mathbf{a}), \\ f_f = E_f(x_t^f), \\ f_b = E_b(x_t^b), \end{cases} \quad (9)$$

where f_a represents the audio feature embedding, with E_a being a pre-trained audio encoder [11], while E_f and E_b are encoders for the face and body motion features, f_f and f_b , respectively. Finally, the output of the first stage is expressed as

$$\hat{x}_0 = D_{\text{SMGA}}(f_f, f_b, f_a, t), \quad (10)$$

where t represents the temporal embedding. These features are subsequently fed into the Spatial Mask-Guided Audio Pose Generation (SMGA) Network, denoted as D_{SMGA} , which decodes them to produce a sequence of audio-driven poses \hat{x}_0 . The generated pose sequence \hat{x}_0 is then visualized as the pose video V_P .

Motion Mask Generation. As depicted in Algorithm 1, our approach introduces a novel method for generating motion masks based on keypoints, represented as $P \in \mathbb{R}^{T \times C_p}$. Here, $C_p = C_f + C_h + C_l$ corresponds to face, hand gestures, and lips, respectively. For each frame within a video sequence, our algorithm transforms normalized keypoint coordinates into pixel coordinates and calculates bounding boxes for designated sections. These bounding boxes are then utilized to construct binary masks, setting active regions to a value of 255. The generated masks include V_M^f for face, V_M^l for limb movements, and V_M^h for hand gestures. Notably, as the head and hand masks are non-overlapping, they are combined into a single mask, denoted as V_M^{f+h} , and we set the background mask to $V_M^b = (255 - V_M^{f+h})$.

Details of the SMGA Network Structure. The SMGA network is carefully designed to capture the temporal and semantic relationships between motion features and audio input. As shown in Fig. 4, its architecture consists of two motion blocks and a merging module. The two motion blocks process the input features f_f or f_b that represent different body parts separately through a combination of self-attention, FiLM (Feature-wise Linear Module), and cross-attention mechanisms to capture the correlation between different body parts and audio. Among them, the self-attention mechanism

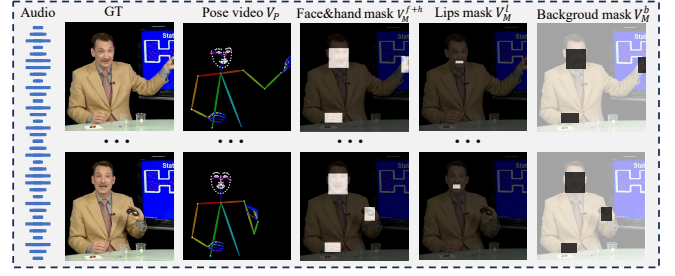


Fig. 5: The details of inputs during model training.

is used to capture the correlation of the motion features themselves, and the calculation formula is as

$$\text{Att}(Q_f, K_f, V_f) = \text{softmax} \left(\frac{Q_f K_f^T}{\sqrt{d_k}} \right) V_f, \quad (11)$$

where Q_f , K_f , V_f are derived from motion features (f_f or f_b). Then, the cross-attention mechanism in different motion modules will capture the different correlations between different body parts and audio embeddings. The specific formulas are as

$$\text{Att}(Q_f, K_{f_a}, V_{f_a}) = \text{Softmax} \left(\frac{Q_f K_{f_a}^T}{\sqrt{d_k}} \right) V_{f_a}, \quad (12)$$

where Q_f is derived from motion features (f_f or f_b), and K_{f_a} , V_{f_a} are derived from the audio features f_a . Through this distraction mechanism, we achieve coherent and coordinated speech actions for different semantic regions (e.g., body and face). In addition, the introduced FiLM layer plays a key role by dynamically adjusting the action features according to the audio embedding, thereby facilitating precise cross-modal alignment.

To ensure the coordination of head movements and hand gestures, the network employs a fusion strategy. First, a multi-layer perceptron (MLP) combines the features of the head movements and hand gestures. Then, a FiLM layer is used to dynamically adapt the fused features. This process is mathematically expressed as

$$f_{\text{merged}} = \text{FiLM}(\text{MLP}(f_f + f_b)), \quad (13)$$

where f_f and f_b represent the head and gesture motion features, respectively. The final dynamic feature map, f_{merged} , is then used to predict the pose sequence \hat{x}_0 , which corresponds to the audio-driven pose sequence. Through this multi-step integration, the model can generate a pose sequence that is highly consistent with the input audio and motion features, and is also temporally coherent and semantically rich.

Loss Function. The training process optimizes the SMGA network using a multi-component loss function to ensure accurate motion generation. The reconstruction loss is defined as

$$\mathcal{L}_{\text{rec}} = \frac{1}{T} \sum_{t=1}^T \|x_t - \hat{x}_t\|_2^2, \quad (14)$$

Algorithm 1 Motion Mask Generator $G_M(\cdot)$

Input: Pre-keypoints $\hat{P} \in \mathbb{R}^{N \times C_p}$, $C_p = (C_f + C_h + C_l)$

Output: Masks videos $V_M^f, V_M^l, V_M^h \leftarrow V_M \in \mathbb{R}^{N \times H \times W}$

```
1: Initialization  $V_M \leftarrow \mathbf{0}$ 
2: for each frame  $t = 1$  to  $N$  do
3:    $bbox \leftarrow \text{None}$ 
4:    $p_i \leftarrow \hat{P}[t]$ 
5:   Initialize  $min_x, min_y \leftarrow W, H$ ,  $max_x, max_y \leftarrow 0, 0$ 
6:   for each  $p_i \in p_i$  do
7:      $x, y \leftarrow \text{int}(p_i \cdot [W, H])$ 
8:     if  $x > 0$  and  $y > 0$  then
9:       Update  $min_x, min_y, max_x, max_y$ 
10:    end if
11:  end for
12:  if  $min_x < max_x$  and  $min_y < max_y$  then
13:     $V_M[t, min_y : max_y, min_x : max_x] \leftarrow 255$ 
14:  end if
15: end for
16: return  $V_M^f, V_M^l, V_M^h$ 
```

where x_t and \hat{x}_t represent the ground-truth and predicted motion features, respectively. The velocity loss is

$$\mathcal{L}_{\text{vel}} = \frac{1}{T-1} \sum_{t=1}^{T-1} \|(x_{t+1} - x_t) - (\hat{x}_{t+1} - \hat{x}_t)\|_2^2. \quad (15)$$

The acceleration loss is expressed as

$$\mathcal{L}_{\text{acc}} = \frac{1}{T-2} \sum_{t=1}^{T-2} \left\| (x_{t+2} - 2x_{t+1} + x_t) - (\hat{x}_{t+2} - 2\hat{x}_{t+1} + \hat{x}_t) \right\|_2^2. \quad (16)$$

Each loss term for head and gesture motion can be defined as

$$\mathcal{L}_f = \mathcal{L}_{\text{rec}}^f + \mathcal{L}_{\text{vel}}^f + \mathcal{L}_{\text{acc}}^f, \quad \mathcal{L}_b = \mathcal{L}_{\text{rec}}^b + \mathcal{L}_{\text{vel}}^b + \mathcal{L}_{\text{acc}}^b. \quad (17)$$

where \mathcal{L}_f and \mathcal{L}_b correspond to the losses for head and gesture motion, respectively. Further details of the reconstruction, velocity, and acceleration terms can be expanded based on the specific metrics used for evaluation. The total loss is computed as

$$\mathcal{L}_{\text{SMGA}} = \lambda_f \mathcal{L}_f + \lambda_b \mathcal{L}_b, \quad (18)$$

where $\lambda_f = 3$ and $\lambda_b = 1$ are weighting factors for the head and gesture motion losses. These weights control the relative contribution of each motion type to the overall optimization process.

C. Motion-Driven Detail Refinement Video Generate

Conditional Input Preparation. The video generation process is initiated by preparing the conditional inputs. As depicted in Fig. 5, the training inputs consist of the audio signal a , the original video V , the pose video V_P , and three

types of motion masks: V_M^{f+h} , V_M^l , and V_M^b . These inputs collectively provide the necessary information to guide the generation of the final video output. We extract a 12-frame video clip from the training set to represent a single step of the model, with the first frame of the clip designated as the reference image I_0 . This reference image serves as the foundational visual context for subsequent processing and generation within the model.

The CLIP [42] image encoder E_{clip} extracts semantic features Z_{text} from the text associated with the reference image I_0 , while the autoencoder E_{vae} [43], [44] encodes the implicit visual representation of the image. For the audio input a , we utilize E_a [45], [46] to extract the corresponding audio features f_a . For the pose video V_P , a specially designed pose encoder [47] is employed to extract pose features, denoted as Z_{pose} . In addition, motion masks $V_M = \{V_M^{f+h}, V_M^l, V_M^b\}$ of different sizes are generated by Gaussian blurring and resizing operations. These masks are then fed into different layers of the model. All extracted features are temporally aligned to ensure that the generated video is synchronized with the input audio.

Motion Masked Hierarchical Audio Attention. The Motion Mask-based Hierarchical Audio Attention (MM-HAA) module is a critical component in the second stage of our framework, designed to refine motion features by dynamically aligning spatial details, motion masks, and audio features. Unlike fixed-mask methods employed in prior works [21], MM-HAA leverages motion motion masks, V_M^{f+h} , V_M^l , and V_M^b which are derived from keypoints generated in the first stage. These masks adaptively focus attention on specific regions, with V_M^{f+h} focusing on face and gestures, V_M^l focusing on lip movements, and V_M^b focusing on the background area. Using a mechanism of cross-attention, MM-HAA aligns intermediate hidden states Z_{CA} with specific temporal and frequency audio characteristics f_a , ensuring spatial-temporal synchronization. The key operation in MM-HAA is modeled as

$$\text{Att}(Q_{Z_{CA}}, K_{f_a}, V_{f_a}) = \text{Softmax} \left(\frac{Q_{Z_{CA}} K_{f_a}^\top}{\sqrt{d_k}} \right) V_{f_a}, \quad (19)$$

where $Q_{Z_{CA}} = W_q Z_{CA}$, $K_{f_a} = W_k f_a$, and $V_{f_a} = W_v f_a$ are the query, key, and value matrices, respectively, and d_k represents the SMGA factor for stability. MM-HAA further integrates these aligned features with the motion masks to enhance region-specific refinement. The masked hidden states are computed as

$$Z'_{f+h} = Z_{CA} \odot V_M^{f+h}, \quad (20)$$

$$Z'_l = Z_{CA} \odot V_M^l, \quad (21)$$

$$Z'_b = Z_{CA} \odot V_M^b. \quad (22)$$

where \odot denotes element-wise multiplication. These masked representations are processed through convolution-based

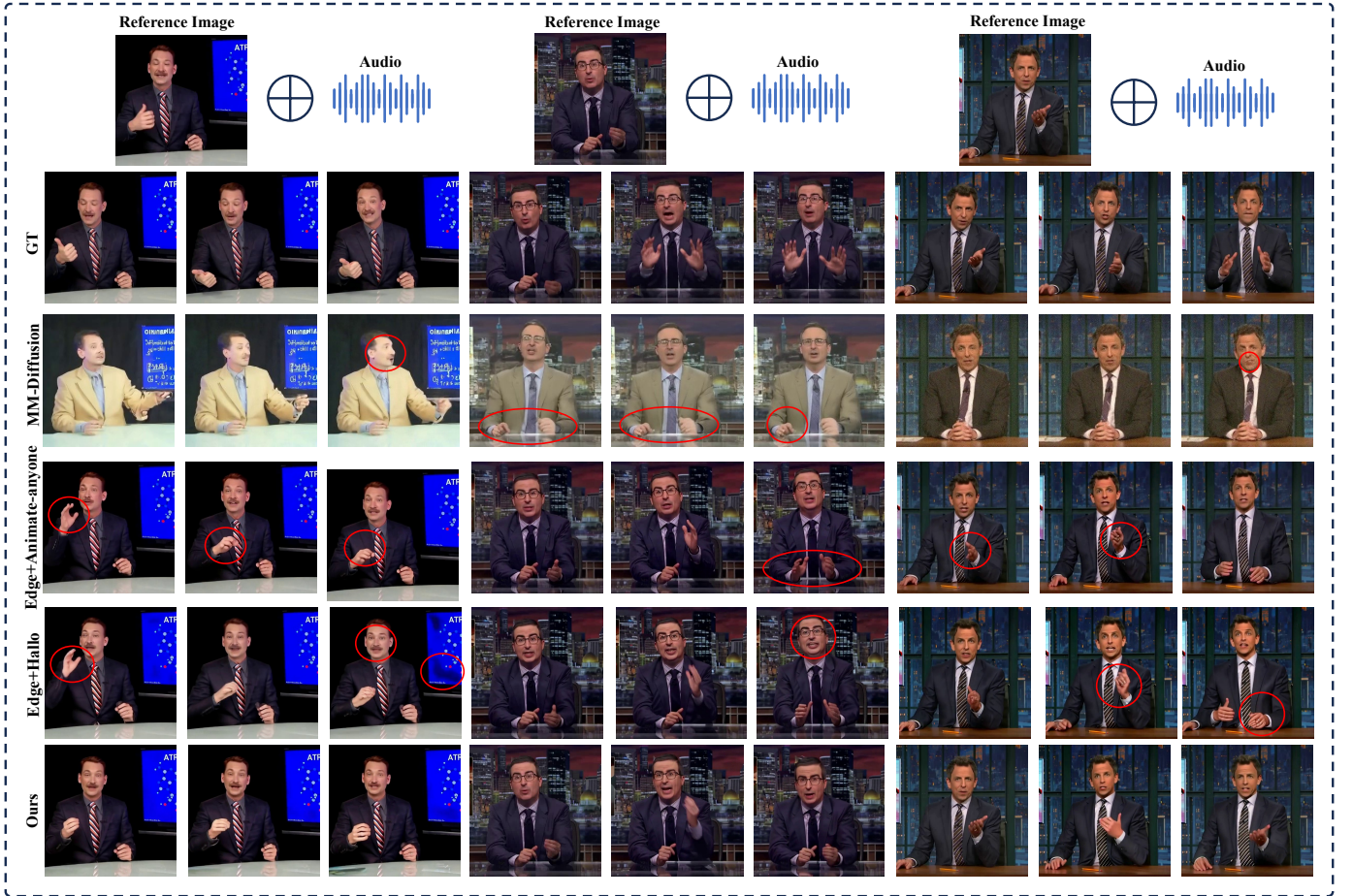


Fig. 6: Qualitative Comparison of Upper Body Speech-Driven Video Generation Models on the PATS Dataset. This figure compares the performance of different speech-driven video generation models (MM-Diffusion [2], EDGE + Animate-anyone [47], [48], EDGE + halo [21], [48] and Ours MMGT) in generating realistic upper-body movements, speech synchronization, and maintaining video quality.

adapter modules, which utilize residual connections and convolutional layers to enhance feature richness

$$Z_{\text{MM-HAA}} = \text{Adapter}_{f+h}(Z'_{f+h}) + \text{Adapter}_l(Z'_l) + \text{Adapter}_b(Z'_b), \quad (23)$$

where Adapter_{f+h} , Adapter_l , and Adapter_b are the convolution-based refinement modules for V_M^{f+h} , V_M^l , and V_M^b respectively.

This combined output $Z_{\text{MM-HAA}}$ is passed to the Temporal Attention (TA) layers in the Denoising UNet, enabling further temporal refinement. The hierarchical design of MM-HAA ensures precise integration of motion masks, audio features, and spatial details across frames. By combining cross-attention and mask-based refinement, the module aligns audio-driven dynamics with spatially localized regions, effectively addressing the limitations of fixed-mask methods. Experimental results demonstrate that MM-HAA significantly improves realism, synchronization, and expressiveness in generated co-speech videos. Its contributions to temporal coherence and region-specific enhancement are essential to the overall success of the proposed framework.

Loss function. The model is optimized using a diffusion-based reconstruction loss

$$\mathcal{L}_{\text{rec}}^{\text{latent}} = \frac{1}{T} \sum_{t=1}^T \|Z_t - \hat{Z}_t\|_2^2, \quad (25)$$

where T represents the number of time steps, Z_t is the generated latent representation at time step t , and \hat{Z}_t is the corresponding target latent representation. The final video \hat{V} is reconstructed by decoding the refined latent representations Z_t through the decoder D_{vae} , which transforms the latent space back into actual video frames.

IV. EXPERIMENTS

A. Experimental setup

Datasets. Our study uses the PATS dataset [27]–[29], which includes 84,000 clips from 25 speakers, averaging 10.7 seconds per clip and totaling 251 hours. We focused on a subset of four speakers (Jon, Kubinec, Oliver, and Seth), extracting 1,200 valid clips per speaker, for a total of 4,800 clips. Using a 0.5s step, we generated 3.2s clip, resulting in 58,844 training clips and 2,048 test clips.

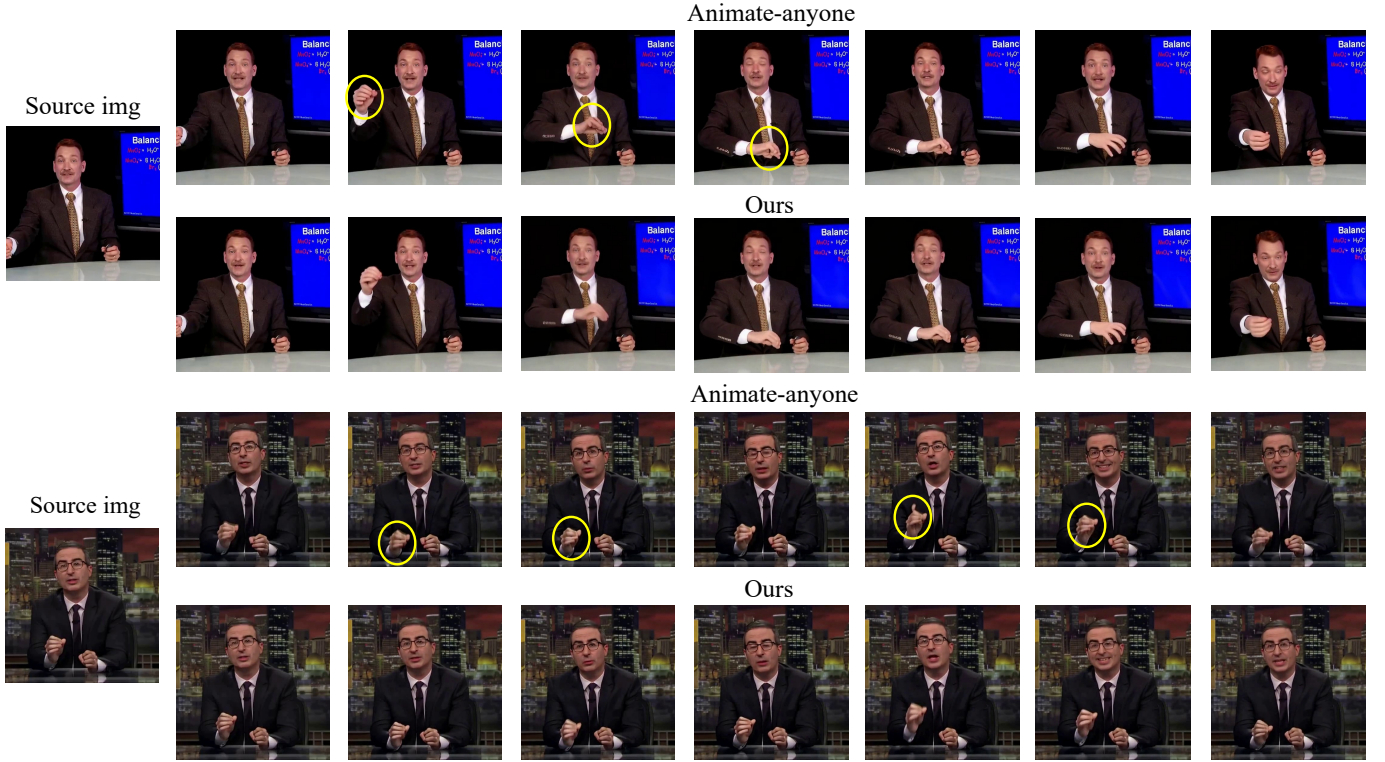


Fig. 7: Qualitative Comparison of Pose-driven Video Generation. This figure compares videos generated by our method and Animate-anyone [47] in a pose-driven task. In contrast, our method achieves high-quality generation with accurate and consistent hand movements.

Evaluation Metrics. The Fréchet Gesture Distance (FGD) [49] is employed to measure the distribution gap between real and generated gestures in the feature space, while Diversity (Div.) [50] quantifies the variability of the generated gestures. Both metrics are computed using an auto-encoder trained on PATS pose data. For evaluating video quality, we leverage Fréchet Video Distance (FVD) [51] and Fréchet Image Distance (FID) with the I3D classifier [52] pre-trained on Kinetics-400 [52]. Furthermore, PSNR [53], SSIM [54] and LPIPS are used to assess pixel-level similarity, ensuring that the generated video closely resembles the ground truth. We also use the SyncNet [55] to calculate **Sync-C** and **Sync-D** for valid the audio-lip synchronization accuracy.

Implementation Details. We train our overall framework on four speakers jointly in two stages. **1)** For the SMGA-Network: We collect keypoints and expand them into motion features $x_0^i \in \mathbb{R}^{402}$ for each frame. For audio feature extraction, we adopt the feature extraction strategy outlined in [11], we set the batch size to 256 and utilize the Adan optimizer with a learning rate of 2×10^{-4} , a weight decay of 0.02, and 3,400 training iterations. The maximum sampling step T is set to 50, and the loss weights In Eq. 18, are configured as $\lambda_f = 3$ and $\lambda_g = 1$. **2)** The multimodal video generation model is trained in two step. The first step comprises 29,580 steps with a batch size of 2, while the second step consists of 32,500 steps with a batch size of 1. Both step share consistent parameter settings, including a video resolution of 512×512 .

To enhance the quality and robustness of video generation, all input modalities are randomly removed with a probability of 5% during the training process. The learning rate for both stages is set to 1×10^{-5} , and optimization is performed using the Adam optimizer. [56].

Experiments encompassing both training and inference were carried out on a computational platform featuring 8 NVIDIA A6000 GPUs. Our training strategy is shown in Algorithm 2. As shown in the Fig.1, in order to make a fair comparison during the inference process, our framework only uses audio and inference images as inputs to the model without introducing other a priori features.

B. Quantitative result

To enhance evaluation efficiency, we standardized the resolution of all videos to 256×256 for assessment. A comprehensive evaluation of various metrics was conducted using a consistent test set to ensure fair and reliable comparisons.

Audio Driver. Currently, open-source training code for audio-driven speech gesture video generation methods is relatively limited, and the training code for some methods, such as [8], [22], [57], [1], and [58], is not publicly available, preventing direct comparisons on the same dataset. To evaluate the advantages of our approach, we modify and integrate some of the existing algorithms, adapting them to the task at hand, and perform uniform training and inference using the same training and test sets.



Fig. 8: Lips Synchronization with Audio. A comparison of lip synchronization with audio across Ground Truth, MM-Diffusion [2], EDGE + Animate-anyone [47], [48], EDGE + Hallo [21], [48], our MMGT model, and our ablation model (MMGT w/o SMGA).

TABLE I: Quantitative comparison of speech-driven gesture video generation methods in terms of gesture, face, lip and overall video quality metrics. This table compares the performance of our proposed method with baseline models (MM-Diffusion [2], EDGE + Animate-anyone [47], [48], EDGE + halo [21], [48] in audio-driven and pose-driven video generation tasks.

Method	Gesture		Face						Lip		Videos				
	FGD(↓)	Div.(↑)	FID(↓)	FVD(↓)	KVD(↓)	PSNR(↑)	SSIM(↑)	LPIPS(↓)	Syn-C(↓)	Syn-D(↑)	FID(↓)	FVD(↓)	PSNR(↑)	SSIM(↑)	LPIPS(↓)
MM-Diffusion [2]	141.76	0.0998	39.28	693.311	63.150	27.94	0.1312	0.6112	13.75	0.82	86.18	1007.01	27.93	0.1667	0.7058
EDGE.+Animate-anyone [47], [48].	<u>6.72</u>	<u>0.0855</u>	<u>4.20</u>	<u>176.915</u>	<u>17.36</u>	<u>29.76</u>	<u>0.4188</u>	<u>0.2670</u>	12.27	2.01	6.91	410.92	<u>31.16</u>	<u>0.6152</u>	<u>0.2374</u>
EDGE.+Hallo [21], [48].	7.57	0.0846	5.72	245.095	24.172	29.54	0.4158	0.2695	<u>12.09</u>	<u>2.28</u>	8.66	<u>398.10</u>	30.44	0.6056	0.2405
Ours(Audio driven)	6.02	0.0824	3.43	99.38	10.49	29.87	0.4413	0.2535	10.16	4.51	<u>7.90</u>	230.89	31.29	0.6378	0.2305

TABLE II: Quantitative Comparison of Video-Driven Gesture Video Generation Methods in Terms of Gesture, Face, Lip, and Overall Video Quality Metrics. This table compares the performance of our proposed method with baseline models Animate-anyone [47] in pose video-driven video generation tasks.

Method	Face						Videos				
	FID(↓)	FVD(↓)	KVD(↓)	PSNR(↑)	SSIM(↑)	LPIPS(↓)	FID(↓)	FVD(↓)	PSNR(↑)	SSIM(↑)	LPIPS(↓)
Animate-anyone [47]	3.11	101.43	9.849	31.50	0.8231	0.1018	4.97	160.20	32.51	0.8105	0.1252
Ours	2.96	84.24	8.531	31.59	0.8315	0.0982	4.72	135.00	32.62	0.8168	0.1225

We constructed two benchmark models of two-stage speech-driven upper body speaking based on current state-of-the-art algorithms such as EDGE [48], Animate-anyone [47] and Hallo [21]. In making modifications to EDGE [48], we refer to S2G-MDD [11] scheme to adapt it to the current dataset. First, we use DWPose [41] to extract the keypoint sequences on the PATS dataset [27]–[29] and construct a paired dataset of gesture sequences and audio as training data for EDGE [48]. For Hallo [21], we add a pose-driven pose guider [47] to it so that it can introduce pose videos during training. In terms of mask acquisition, since Hallo [21] can only acquire static masks for faces, and faces in speech videos are small and cannot acquire masks efficiently, we adjusted the mask acquisition method by using YOLOv5 [59] to acquire static masks for different regions of the human body, making it more suitable for the task of generating videos of the upper half of

the body.

In the second phase, we train Animate-anyone [47] using pose videos and GT videos, while we train Hallo [21] using pose videos, GT videos, and audio. In terms of inference, we use the same test set, first generating videos of DWPose keypoints [41] using EDGE, and then using these keypoints for each of Hallo [21] and Animate-anyone [47] video rendering respectively.

As shown in Table I, our method significantly outperforms other approaches in overall video quality. Specifically, our FVD score improves from 398.10 (for EDGE+Hallo) to 230.89, highlighting a notable enhancement. Moreover, our model achieves the best results in key metrics such as PSNR, SSIM, and LPIPS. In lip synchronization, our method excels with superior performance in both Syn-C and Syn-D metrics. For facial quality, our approach also delivers the best results. In

Algorithm 2 Training Algorithm

Input: Reference image I_0 , Driven audio a , and GT-video V ,
 θ_1, θ_2 are parameters of D_{SMGA}, D_{LV}

Output: The optimal parameters θ_1^*, θ_2^*

```

1: Stage 1 Input Preparation
2:  $x_0 \leftarrow E_K(V) = \{p^0, \dots, p^L\} \triangleright \mathbb{R}^{L \times C}$ 
3:  $x_r \leftarrow \text{repeat}((E_K(I_0))) = \{p^0, \dots, p^0\} \triangleright \mathbb{R}^{L \times C}$ 
4:  $m_{body} = [0, 1] \in \mathbb{R}^{L \times C_b}$ 
5:  $M = \{m_{body}, 1 - m_{body}\}$ 
6:  $x_t \leftarrow \text{concat}(x_0 + \mathcal{N}(0, \sigma^2), x_r)$ 
7:  $\mathbf{c}_1 = \{M, x_t, E_a(a)\}$ 
8: Stage 2 Input Preparation
9:  $z_0 \leftarrow E_{vae}(V) \triangleright \mathbb{R}^{L \times C \times H \times W}$ 
10:  $z_t \leftarrow z_0 + \mathcal{N}(0, \sigma^2)$ 
11:  $V_M = G_M(x_0)$  {based on Algorithm.1}
12:  $V_P = \text{Visualization}(x_0)$ 
13:  $\mathbf{c}_2 = \{I, V_M, V_P, E_a(a)\}$ 
14: Training
15: repeat
16:   Sample  $t \sim \text{Uniform}(\{1, \dots, T\})$ 
17:    $\mathcal{L}_{SMGA} \leftarrow \text{Loss}(D_{SMGA}(\mathbf{c}_1), x_0)$  {based on Eq.18}
18:    $\theta_1 \leftarrow \theta_1 - \nabla_{\theta_1}(\mathcal{L}_{SMGA}, l_G)$ 
19:    $\mathcal{L}_{GLV} \leftarrow \text{Loss}(D_{LV}(\mathbf{c}_2), z_0)$  {based on Eq.25}
20:    $\theta_2 \leftarrow \theta_2 - \nabla_{\theta_2}(\mathcal{L}_{GLV}, l_D)$ 
21:    $= \theta_2 - \nabla_{\theta_2} \|\epsilon - \epsilon_{\theta_2}(\sqrt{\alpha_t}z_0 + \sqrt{1 - \alpha_t}\epsilon, \mathbf{c}_2, t)\|^2$ 
22: until converged
23:  $id_{\min} \leftarrow \text{Argmin}([rmse_i])$  {the  $id$  of the min values}
24:  $\theta_1^* \leftarrow [\theta_1^i](id_{\min}), \theta_2^* \leftarrow [\theta_2^i](id_{\min})$ 

```

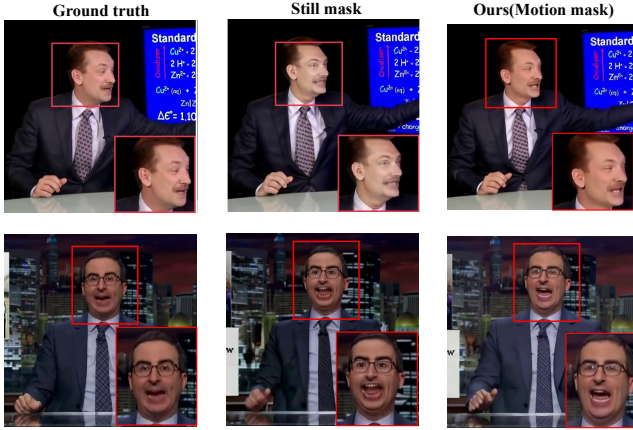


Fig. 9: Qualitative Comparison of Video Generation with Still and Motion Masks.

terms of gesture generation, we achieve a clear improvement in the FGD metric. Although the Div metric may not accurately reflect pose generation quality when significant jitter is present, it is less indicative in this context. This is further demonstrated in the qualitative experiments.

Pose video-driven generation. We adapted the approach

by replacing the audio-driven pose videos with whole-body keypoint sequences extracted from the PATS dataset [27]–[29] using DWPose [41] during the inference process for the video-driven gesture generation task. As shown in Table II, our method outperforms the current state-of-the-art method, Animate-anyone [47], across multiple evaluation metrics, including FID, FVD, PSNR, SSIM, and LPIPS, for both the overall video quality and the facial region. Specifically, our model shows improvements in FID, FVD, and LPIPS, achieving better perceptual similarity and video coherence. Furthermore, the visual results presented in Fig. 7 demonstrate that our approach, MMGT, excels in maintaining structural integrity and identity consistency, especially in localized regions like hands.

C. Qualitative results.

Qualitative Comparative Experiment. We show a qualitative comparison of the upper body speech-driven video generation model on the PATS dataset, as seen in Fig. 6, where EDGE + Animate-anyone [47], [48] hand movements are delayed and unnatural, and lip synchronization is not aligned. edge + hallo [21], [48] face There is noticeable distortion, hand distortion, and a lot of artifacts in the background. In contrast, our proposed method generates videos that are closer to GT, with more natural and synchronized gestures, accurate lip alignment, and no artifacts in the background.

We also demonstrate a qualitative comparison of video generation models driven by upper body pose videos on the PATS dataset, as shown in Fig. 7, where Animate-anyone [47] generated video fails to maintain consistency with ground truth in the hand region. In contrast, our approach yields more accurate and visually consistent results, effectively maintaining the integrity of facial and hand movements.

Lips Synchronization with Audio. For the qualitative comparison of lip synchronization, Fig. 8 illustrates the lip synchronization results for the word ‘negative’ in the audio phrase. Our method (MMGT) produces lip shapes that are closely aligned with the Ground Truth, accurately capturing both the timing and subtle dynamics of the word. In contrast, EDGE + Animate-anyone [47], [48] and MM-Diffusion [2] show noticeable mismatches in lip movements, resulting in poor synchronization with the audio. EDGE + Hallo [21], [48] exhibits large distortions and artifacts in the lips. Our ablation model (MMGT w/o SMGA), the generated lip shape is nearly stationary and significantly deviates from the ground truth. Additionally, we provide quantitative metrics for lip synchronization in Table I and Table III, which include Syn-C and Syn-D to evaluate synchronization accuracy and diversity, respectively. The results further validate the robustness and superiority of our method over the baseline and ablation variants.

Effectiveness of Motion Masks in Video Generation. Fig. 9 illustrates the qualitative comparison of video generation results under the same input conditions using still masks and motion masks. Two representative frames are selected to showcase the effectiveness of the proposed method. As shown,

TABLE III: The quantitative results of the ablation study highlight the impact of the key modules on gesture generation, video quality and audiovisual synchronization metrics.

Method	Gesture		Face						Lip		Videos				
	FGD(↓)	Div.(↑)	FID(↓)	FVD(↓)	KVD(↓)	PSNR(↑)	SSIM(↑)	LPIPS(↓)	Syn-C(↓)	Syn-D(↑)	FID(↓)	FVD(↓)	PSNR(↑)	SSIM(↑)	LPIPS(↓)
w/o SMGA	6.78	0.0813	17.99	262.20	25.01	29.42	0.3775	0.3250	11.83	2.25	17.91	409.532	30.42	0.5876	0.2735
w/o \mathcal{L}_f	7.09	0.0772	5.12	<u>167.58</u>	<u>16.40</u>	29.45	0.3943	0.2877	11.16	3.18	11.49	411.415	30.54	0.6039	0.2544
w/o Motion Mask	6.51	0.0831	<u>4.24</u>	205.08	29.70	29.57	0.4267	0.2618	<u>10.18</u>	4.65	<u>9.30</u>	378.32	30.32	0.6108	0.2380
w/o Audio	6.72	0.0824	21.50	609.44	30.04	<u>29.67</u>	<u>0.4315</u>	<u>0.2553</u>	11.03	3.58	31.56	1250.71	<u>30.80</u>	<u>0.6237</u>	<u>0.2347</u>
w Still Mask	7.09	0.0833	5.35	267.10	25.46	29.42	0.3775	0.3250	10.84	4.01	9.71	286.389	30.28	0.6050	0.2430
Ours(Ours)	6.02	0.0825	3.43	99.38	10.49	29.87	0.4413	0.2535	10.16	<u>4.51</u>	7.90	230.89	31.29	0.6378	0.2305

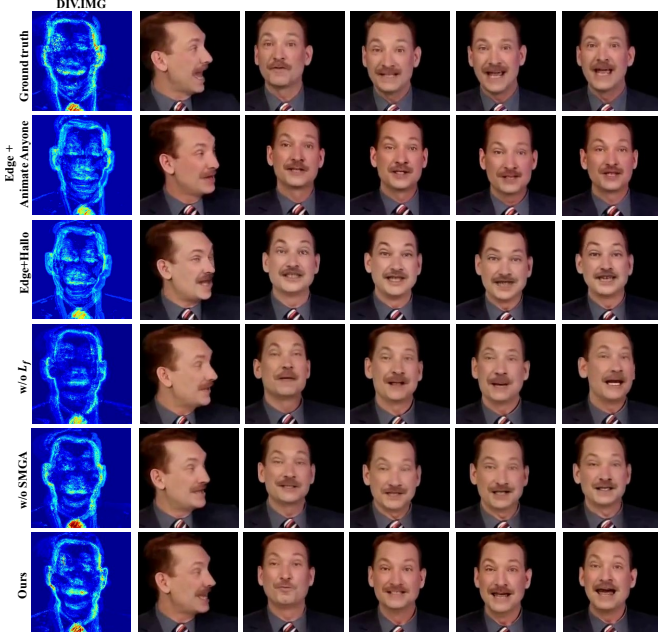


Fig. 10: Presentation and qualitative comparison of overall head diversity maps based on the PATS dataset

the incorporation of motion masks leads to significant improvements in the generated video quality, particularly in the facial and lip regions, where finer details and movement synchronization are better captured. By leveraging the dynamic information provided by motion masks, the model generates more realistic and coherent videos compared to using still masks. To provide a comprehensive assessment, we further validate these observations through ablation experiments using quantitative metrics, as shown in Table III.

Evaluation of Facial Motion Diversity and Synchronization. We conducted a detailed comparison of facial motion diversity and synchronization for individual test videos, evaluating Ground Truth, EDGE + Animate-anyone [47], [48], EDGE + Hallo [21], [48], our method MMGT, and the ablation version of our method (MMGT w/o SMGA and MMGT w/o \mathcal{L}_f). As shown in Fig. 10, the motion diversity heatmap (DIV-IMG) on the left side visualizes the magnitude of the motions, where blue represents the smallest motions, green and yellow indicate moderate motions, and red highlights the

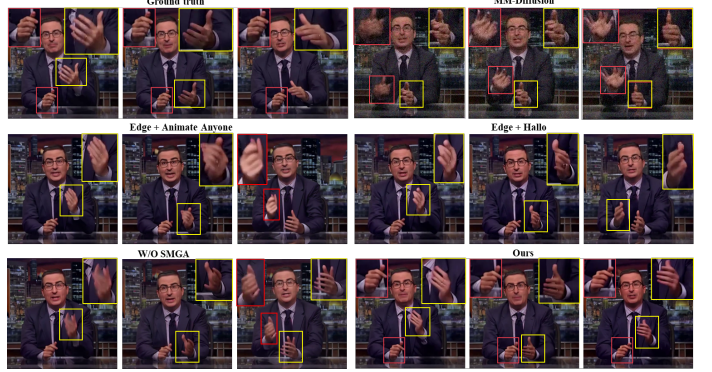


Fig. 11: Hands Detailed Comparisons. Detailed comparisons of hand motion among MM-Diffusion [2], EDGE + Animate-anyone [47], [48], EDGE + Hallo [21], [48], our MMGT model, and our ablation model (MMGT w/o SMGA).

most significant motions. From the comparison of the diversity maps, our method captures the most pronounced and accurate lip movements that closely match the ground truth.

The qualitative comparison on the right further highlights the differences between the various methods. Our approach not only generates accurate and well-synchronized lip shapes, but also preserves subtle micro-expressions, resulting in output that closely matches the Ground Truth. In contrast, the variant without SMGA exhibits almost no lip movement, underscoring the critical role of the SMGA module in achieving precise lip synchronization with the audio. Similarly, the ablated model w/o \mathcal{L}_f , which lacks the facial loss function, produces rigid face and less distinct lip motion, underscoring the importance of the facial loss for natural expression generation. EDGE + Animate-anyone [47], [48] and EDGE + Hallo [21], [48] struggle to generate synchronized lips with detailed facial movements. In comparison, our method excels in both motion diversity and quality. These results clearly validate the effectiveness of our full model design in generating realistic, synchronized upper-body videos.

Detailed Comparison of Hand Motion Across Methods. We highlight the performance of different methods in reproducing hand motion. As shown in Fig. 11, MM-Diffusion [2] generates noticeable artifacts and blurred hand shapes, failing to capture the fine details and consistency of hand movements. Similarly, EDGE + Animate-anyone [47], [48] and EDGE

+ Hallo [21], [48] struggle with accurate hand positioning and shape generation, resulting in significant discrepancies from the Ground Truth. In contrast, our method demonstrates superior fidelity, accurately capturing realistic hand gestures with precise motion and clear structural details, closely aligning with the Ground Truth. This comparison emphasizes the effectiveness of our method in generating coherent and visually accurate hand motions in video synthesis.

D. Ablation Study.

We conducted ablation studies on the PATS dataset to evaluate the influence of key components in our framework, with the quantitative results presented in Table III. In this table, "w/o SMGA" indicates the replacement of our SMGA network with a baseline keypoint generation method (EDGE [48]), "w/o (\mathcal{L}_f)" corresponds to removing the facial loss (\mathcal{L}_f) in the first stage, "w/o Motion Mask" signifies the omission of the motion mask in the MM-HAA module, and "w/o Audio" replaces audio cross-attention with self-attention to negate the effect of audio inputs.

We replaced the dual-motion block in the SMGA network with a single-motion block while using x_t as input to the ablation network in the first stage, which resulted in a significant decrease in lip synchronization and overall motion quality. As shown in Table III, the Syn-C metric increased significantly from 10.16 to 11.83, indicating a decrease in the credibility of lip synchronization, and the Syn-D metric increased from 4.51 to 5.38, reflecting a weakening of the temporal consistency of lip movements. Gesture and facial quality also decreased, as evidenced by higher FGD and FVD scores, highlighting the importance of SMGA in maintaining robust lip synchronization (Fig.11 and Fig.10).

Similarly, substituting the motion-specific facial loss \mathcal{L}_f with a generalized loss leads to a pronounced decrease in lip synchronization accuracy. The Syn-C metric rises from 10.16 to 11.11, and the Syn-D metric increases from 4.51 to 4.65, signifying diminished articulation precision and temporal coherence between the lips and audio. As shown in Fig. 10, this degradation visibly manifests as weaker lip movements aligned with the spoken content.

Eliminating the motion mask in the MM-HAA module further degrades performance. The facial FVD score increases to 205.08, while the overall video FVD soars to 378.32, indicating deteriorating temporal coherence and video fidelity. Moreover, metrics related to facial detail (PSNR, KVD, and LPIPS) also show declines, indicating loss of detail and perceptual quality. Although lip synchronization remains relatively stable—thanks to shared pose-driven inference—the enhancements in other metrics reaffirm the value of dynamic masking for preserving both global video quality and fine-grained details.

Removing the audio input entirely and relying solely on keypoint-driven generation leads to substantial performance drops in both facial and overall metrics (e.g., FVD and FID), emphasizing the essential role of audio in enhancing visual

quality and temporal consistency. Furthermore, the notable decrease in lip synchronization highlights the necessity of audio-based guidance for achieving realistic, accurate lip movements.

When a static mask replaces the motion mask in the MM-HAA module, face-specific metrics such as SSIM and PSNR decrease (from 0.3945 to 0.3775 and from 29.47 to 29.42, respectively), while the facial FVD score increases from 99.38 to 267.10, indicating a marked loss of detail in the face region. Gesture coherence also degrades (FGD rises from 7.04 to 7.089), and the overall video FVD increases from 230.89 to 286.389, pointing to diminished temporal consistency and video quality (Fig. 9).

Collectively, these ablation studies highlight the crucial roles played by the SMGA network, the motion-specific facial loss \mathcal{L}_f , the motion mask, and audio-based guidance. Each component significantly contributes to generating high-quality, semantically rich, and temporally coherent facial and gesture videos, as demonstrated by the superior performance of the **MMGT** network.

E. Ethical Considerations and Mitigation Strategies

This study identifies two key societal risks in audio-driven portrait animation technology: potential misuse for creating deceptive deepfakes and privacy violations through unauthorized use of personal biometric data. Addressing these concerns requires establishing ethical guidelines, ensuring transparent deployment, securing explicit user consent, and implementing robust data governance. These measures aim to align technological development with social accountability while promoting socially beneficial applications.

V. CONCLUSIONS.

We propose a Motion Mask-Guided Two-Stage Network (MMGT) for Co-Speech Gesture Video Generation, integrating motion masks and features extracted from audio. The Spatial Mask-Guided Audio Pose Generation (SMGA) network captures large-scale facial and gesture movements, while the Motion Masked Hierarchical Audio Attention (MM-HAA) mechanism refines fine-grained details within a stabilized diffusion framework. Experiments show that MMGT produces natural, high-quality videos with enhanced motion realism and texture accuracy.

REFERENCES

- [1] R. Meng, X. Zhang, Y. Li, and C. Ma, "Echomimicv2: Towards striking, simplified, and semi-body human animation," *arXiv preprint arXiv:2411.10061*, 2024.
- [2] L. Ruan, Y. Ma, H. Yang, H. He, B. Liu, J. Fu, N. J. Yuan, Q. Jin, and B. Guo, "Mm-diffusion: Learning multi-modal diffusion models for joint audio and video generation," in *CVPR*, 2023.
- [3] G. Lin, J. Jiang, C. Liang, T. Zhong, J. Yang, and Y. Zheng, "Cyberhost: Taming audio-driven avatar diffusion model with region codebook attention," *arXiv preprint arXiv:2409.01876*, 2024.
- [4] S. Goldin-Meadow, "The role of gesture in communication and thinking," *Trends in cognitive sciences*, vol. 3, no. 11, pp. 419–429, 1999.
- [5] J. K. Burgoon, T. Birk, and M. Pfau, "Nonverbal behaviors, persuasion, and credibility," *Human communication research*, vol. 17, no. 1, pp. 140–169, 1990.

- [6] Z. Niu, K. Lu, J. Xue, X. Qin, J. Wang, and L. Shao, "From methods to applications: A review of deep 3d human motion capture," *IEEE Transactions on Circuits and Systems for Video Technology*, vol. 34, no. 11, pp. 11 340–11 359, 2024.
- [7] P. Pataranutaporn, V. Danry, J. Y. Y. Leong, P. Punpongsanon, D. Novy, P. Maes, and M. Sra, "Ai-generated characters for supporting personalized learning and well-being," *Nature Machine Intelligence*, vol. 3, pp. 1013 – 1022, 2021. [Online]. Available: <https://api.semanticscholar.org/CorpusID:245238974>
- [8] S. Hogue, C. Zhang, H. Daruger, Y. Tian, and X. Guo, "Diffited: One-shot audio-driven ted talk video generation with diffusion-based co-speech gestures," in *Proceedings of the IEEE/CVF Conference on Computer Vision and Pattern Recognition*, 2024, pp. 1922–1931.
- [9] H. Liu, X. Yang, T. Akiyama, Y. Huang, Q. Li, S. Kuriyama, and T. Take-tomi, "Tango: Co-speech gesture video reenactment with hierarchical audio motion embedding and diffusion interpolation," *arXiv preprint arXiv:2410.04221*, 2024.
- [10] X. Liu, Q. Wu, H. Zhou, Y. Du, W. Wu, D. Lin, and Z. Liu, "Audio-driven co-speech gesture video generation," *Advances in Neural Information Processing Systems*, vol. 35, pp. 21 386–21 399, 2022.
- [11] X. He, Q. Huang, Z. Zhang, Z. Lin, Z. Wu, S. Yang, M. Li, Z. Chen, S. Xu, and X. Wu, "Co-speech gesture video generation via motion-decoupled diffusion model," in *Proceedings of the IEEE/CVF Conference on Computer Vision and Pattern Recognition*, 2024, pp. 2263–2273.
- [12] R. Kumar, J. Sotelo, K. Kumar, A. De Brebisson, and Y. Bengio, "Obamanet: Photo-realistic lip-sync from text," *arXiv preprint arXiv:1801.01442*, 2017.
- [13] A. Creswell, T. White, V. Dumoulin, K. Arulkumaran, B. Sengupta, and A. A. Bharath, "Generative adversarial networks: An overview," *IEEE signal processing magazine*, vol. 35, no. 1, pp. 53–65, 2018.
- [14] K. Prajwal, R. Mukhopadhyay, V. P. Nambodiri, and C. Jawahar, "A lip sync expert is all you need for speech to lip generation in the wild," in *Proceedings of the 28th ACM international conference on multimedia*, 2020, pp. 484–492.
- [15] W. Zhang, X. Cun, X. Wang, Y. Zhang, X. Shen, Y. Guo, Y. Shan, and F. Wang, "Sadtalker: Learning realistic 3d motion coefficients for stylized audio-driven single image talking face animation," in *Proceedings of the IEEE/CVF Conference on Computer Vision and Pattern Recognition*, 2023, pp. 8652–8661.
- [16] L. Tian, Q. Wang, B. Zhang, and L. Bo, "Emo: Emote portrait alive-generating expressive portrait videos with audio2video diffusion model under weak conditions," *arXiv preprint arXiv:2402.17485*, 2024.
- [17] J. Lyu, X. Lan, G. Hu, H. Jiang, W. Gan, J. Wang, and J. Xue, "Multimodal emotional talking face generation based on action units," *IEEE Transactions on Circuits and Systems for Video Technology*, pp. 1–1, 2024.
- [18] Z. Sheng, L. Nie, M. Zhang, X. Chang, and Y. Yan, "Stochastic latent talking face generation toward emotional expressions and head poses," *IEEE Transactions on Circuits and Systems for Video Technology*, vol. 34, no. 4, pp. 2734–2748, 2024.
- [19] R. Rombach, A. Blattmann, D. Lorenz, P. Esser, and B. Ommer, "High-resolution image synthesis with latent diffusion models," in *Proceedings of the IEEE/CVF conference on computer vision and pattern recognition*, 2022, pp. 10 684–10 695.
- [20] H. Wei, Z. Yang, and Z. Wang, "Aniporrait: Audio-driven synthesis of photorealistic portrait animation," *arXiv preprint arXiv:2403.17694*, 2024.
- [21] M. Xu, H. Li, Q. Su, H. Shang, L. Zhang, C. Liu, J. Wang, L. Van Gool, Y. Yao, and S. Zhu, "Hallo: Hierarchical audio-driven visual synthesis for portrait image animation," *arXiv preprint arXiv:2406.08801*, 2024.
- [22] Z. Chen, J. Cao, Z. Chen, Y. Li, and C. Ma, "Echomimic: Lifelike audio-driven portrait animations through editable landmark conditions," *arXiv preprint arXiv:2407.08136*, 2024.
- [23] T. Afouras, J. S. Chung, A. Senior, O. Vinyals, and A. Zisserman, "Deep audio-visual speech recognition," *IEEE transactions on pattern analysis and machine intelligence*, vol. 44, no. 12, pp. 8717–8727, 2018.
- [24] A. Nagrani, J. S. Chung, W. Xie, and A. Zisserman, "Voxceleb: Large-scale speaker verification in the wild," *Computer Speech & Language*, vol. 60, p. 101027, 2020.
- [25] K. Wang, Q. Wu, L. Song, Z. Yang, W. Wu, C. Qian, R. He, Y. Qiao, and C. C. Loy, "Mead: A large-scale audio-visual dataset for emotional talking-face generation," in *European Conference on Computer Vision*. Springer, 2020, pp. 700–717.
- [26] Z. Zhang, L. Li, Y. Ding, and C. Fan, "Flow-guided one-shot talking face generation with a high-resolution audio-visual dataset," in *Proceedings of the IEEE/CVF Conference on Computer Vision and Pattern Recognition*, 2021, pp. 3661–3670.
- [27] C. Ahuja, D. W. Lee, Y. I. Nakano, and L.-P. Morency, "Style transfer for co-speech gesture animation: A multi-speaker conditional-mixture approach," in *Computer Vision–ECCV 2020: 16th European Conference, Glasgow, UK, August 23–28, 2020, Proceedings, Part XVIII* 16. Springer, 2020, pp. 248–265.
- [28] C. Ahuja, D. W. Lee, R. Ishii, and L.-P. Morency, "No gestures left behind: Learning relationships between spoken language and freeform gestures," in *Findings of the Association for Computational Linguistics: EMNLP 2020*, T. Cohn, Y. He, and Y. Liu, Eds. Online: Association for Computational Linguistics, Nov. 2020, pp. 1884–1895. [Online]. Available: <https://aclanthology.org/2020.findings-emnlp.170>
- [29] C. Ahuja, D. W. Lee, Y. I. Nakano, and L. Morency, "Style transfer for co-speech gesture animation: A multi-speaker conditional-mixture approach," *CoRR*, vol. abs/2007.12553, 2020. [Online]. Available: <https://arxiv.org/abs/2007.12553>
- [30] M. Zhang, Z. Cai, L. Pan, F. Hong, X. Guo, L. Yang, and Z. Liu, "Motiondiffuse: Text-driven human motion generation with diffusion model," *arXiv preprint arXiv:2208.15001*, 2022.
- [31] Y. Wang, R. Gao, K. Chen, K. Zhou, Y. Cai, L. Hong, Z. Li, L. Jiang, D.-Y. Yeung, Q. Xu *et al.*, "Detdiffusion: Synergizing generative and perceptive models for enhanced data generation and perception," in *Proceedings of the IEEE/CVF Conference on Computer Vision and Pattern Recognition*, 2024, pp. 7246–7255.
- [32] S. Yang, Z. Wu, M. Li, Z. Zhang, L. Hao, W. Bao, M. Cheng, and L. Xiao, "Diffusestylegesture: Stylized audio-driven co-speech gesture generation with diffusion models," *arXiv preprint arXiv:2305.04919*, 2023.
- [33] K. Chhatre, N. Athanasiou, G. Becherini, C. Peters, M. J. Black, T. Bolkart *et al.*, "Emotional speech-driven 3d body animation via disentangled latent diffusion," in *Proceedings of the IEEE/CVF Conference on Computer Vision and Pattern Recognition*, 2024, pp. 1942–1953.
- [34] H. Liu, Z. Zhu, G. Becherini, Y. Peng, M. Su, Y. Zhou, X. Zhe, N. Iwamoto, B. Zheng, and M. J. Black, "Emage: Towards unified holistic co-speech gesture generation via expressive masked audio gesture modeling," in *Proceedings of the IEEE/CVF Conference on Computer Vision and Pattern Recognition*, 2024, pp. 1144–1154.
- [35] J. Chen, Y. Liu, J. Wang, A. Zeng, Y. Li, and Q. Chen, "Diffshg: A diffusion-based approach for real-time speech-driven holistic 3d expression and gesture generation," in *Proceedings of the IEEE/CVF Conference on Computer Vision and Pattern Recognition*, 2024, pp. 7352–7361.
- [36] Y. Zhou, J. Yang, D. Li, J. Saito, D. Aneja, and E. Kalogerakis, "Audio-driven neural gesture reenactment with video motion graphs," in *Proceedings of the IEEE/CVF conference on computer vision and pattern recognition*, 2022, pp. 3418–3428.
- [37] A. Siarohin, O. J. Woodford, J. Ren, M. Chai, and S. Tulyakov, "Motion representations for articulated animation," in *Proceedings of the IEEE/CVF Conference on Computer Vision and Pattern Recognition*, 2021, pp. 13 653–13 662.
- [38] F. L. Bookstein, "Principal warps: Thin-plate splines and the decomposition of deformations," *IEEE Transactions on pattern analysis and machine intelligence*, vol. 11, no. 6, pp. 567–585, 1989.
- [39] W. Peebles and S. Xie, "Scalable diffusion models with transformers," 2023. [Online]. Available: <https://arxiv.org/abs/2212.09748>
- [40] R. Rombach, A. Blattmann, D. Lorenz, P. Esser, and B. Ommer, "High-resolution image synthesis with latent diffusion models," in *Proceedings of the IEEE Conference on Computer Vision and Pattern Recognition (CVPR)*, 2022. [Online]. Available: <https://github.com/CompVis/latent-diffusionhttps://arxiv.org/abs/2112.10752>
- [41] Z. Yang, A. Zeng, C. Yuan, and Y. Li, "Effective whole-body pose estimation with two-stages distillation," in *Proceedings of the IEEE/CVF International Conference on Computer Vision*, 2023, pp. 4210–4220.
- [42] A. Radford, J. W. Kim, C. Hallacy, A. Ramesh, G. Goh, S. Agarwal, G. Sastry, A. Askell, P. Mishkin, J. Clark *et al.*, "Learning transferable visual models from natural language supervision," in *International conference on machine learning*. PMLR, 2021, pp. 8748–8763.
- [43] D. P. Kingma, "Auto-encoding variational bayes," *arXiv preprint arXiv:1312.6114*, 2013.

- [44] A. Van Den Oord, O. Vinyals *et al.*, “Neural discrete representation learning,” *Advances in neural information processing systems*, vol. 30, 2017.
- [45] A. Baevski, Y. Zhou, A. Mohamed, and M. Auli, “wav2vec 2.0: A framework for self-supervised learning of speech representations,” *Advances in neural information processing systems*, vol. 33, pp. 12 449–12 460, 2020.
- [46] S. Chen, C. Wang, Z. Chen, Y. Wu, S. Liu, Z. Chen, J. Li, N. Kanda, T. Yoshioka, X. Xiao *et al.*, “Wavlm: Large-scale self-supervised pre-training for full stack speech processing,” *IEEE Journal of Selected Topics in Signal Processing*, vol. 16, no. 6, pp. 1505–1518, 2022.
- [47] L. Hu, “Animate anyone: Consistent and controllable image-to-video synthesis for character animation,” in *Proceedings of the IEEE/CVF Conference on Computer Vision and Pattern Recognition*, 2024, pp. 8153–8163.
- [48] J. Tseng, R. Castellon, and K. Liu, “Edge: Editable dance generation from music,” in *Proceedings of the IEEE/CVF Conference on Computer Vision and Pattern Recognition*, 2023, pp. 448–458.
- [49] Y. Yoon, B. Cha, J.-H. Lee, M. Jang, J. Lee, J. Kim, and G. Lee, “Speech gesture generation from the trimodal context of text, audio, and speaker identity,” *ACM Transactions on Graphics (TOG)*, vol. 39, no. 6, pp. 1–16, 2020.
- [50] X. Liu, Q. Wu, H. Zhou, Y. Xu, R. Qian, X. Lin, X. Zhou, W. Wu, B. Dai, and B. Zhou, “Learning hierarchical cross-modal association for co-speech gesture generation,” in *Proceedings of the IEEE/CVF Conference on Computer Vision and Pattern Recognition*, 2022, pp. 10 462–10 472.
- [51] T. Unterthiner, S. Van Steenkiste, K. Kurach, R. Marinier, M. Michalski, and S. Gelly, “Towards accurate generative models of video: A new metric & challenges,” *arXiv preprint arXiv:1812.01717*, 2018.
- [52] J. Carreira and A. Zisserman, “Quo vadis, action recognition? A new model and the kinetics dataset,” in *CVPR*, 2017, pp. 4724–4733.
- [53] A. Hore and D. Ziou, “Image quality metrics: Psnr vs. ssim,” in *2010 20th international conference on pattern recognition*. IEEE, 2010, pp. 2366–2369.
- [54] Z. Wang, A. C. Bovik, H. R. Sheikh, and E. P. Simoncelli, “Image quality assessment: from error visibility to structural similarity,” *IEEE transactions on image processing*, vol. 13, no. 4, pp. 600–612, 2004.
- [55] J. S. Chung and A. Zisserman, “Out of time: Automated lip sync in the wild,” in *ACCV Workshops*, 2016. [Online]. Available: <https://api.semanticscholar.org/CorpusID:26294509>
- [56] D. P. Kingma and J. Ba, “Adam: A method for stochastic optimization,” 2017. [Online]. Available: <https://arxiv.org/abs/1412.6980>
- [57] Y. Zhang, J. Gu, L.-W. Wang, H. Wang, J. Cheng, Y. Zhu, and F. Zou, “Mimicmotion: High-quality human motion video generation with confidence-aware pose guidance,” *arXiv preprint arXiv:2406.19680*, 2024.
- [58] E. Corona, A. Zanfir, E. G. Bazavan, N. Kolotouros, T. Alldieck, and C. Sminchisescu, “Vlogger: Multimodal diffusion for embodied avatar synthesis,” *arXiv preprint arXiv:2403.08764*, 2024.
- [59] J. Redmon, “You only look once: Unified, real-time object detection,” in *Proceedings of the IEEE conference on computer vision and pattern recognition*, 2016.



Jiawei Liu (Member, IEEE) received his B.E. degree from Northeast Agricultural University, Harbin, China, in 2018, and his Ph.D. degree in Pattern Recognition and Intelligent Systems from the Shenyang Institute of Automation, Chinese Academy of Sciences, Shenyang, China, in 2024.

He is currently a research assistant professor at Shenyang Institute of Automation, Chinese Academy of Sciences. His research interests include deep learning, illumination processing, image restoration, shadow removal, and diffusion models.



Yeying Jin (Member, IEEE) received her B.E. degree from the University of Electronic Science and Technology of China (UESTC), and received her M.Sc., Ph.D. degree from the National University of Singapore (NUS).

She is a currently Senior Researcher at Tencent and previously completed a research internship at Adobe, where she was mentored by Prof. Connelly Barnes. Her research interests include computer vision and deep learning, with a focus on image and video generation and enhancement.



Wei Wang received his B.E. degree and M.E. degree from Xidian University, Xi'an, China, In 2014, he received a doctorate degree at Shenyang Institute of Automation, Chinese Academy of Sciences, China.

He is currently an professor at the Shenyang Institute of Automation, Chinese Academy of Sciences, and deputy director of the Intelligent Inspection and Equipment Research Laboratory.



Jinsong Du received his B.E. degree from Shenyang University of Technology, Shenyang, China, in 1993, and his Ph.D. degree in Chinese Academy of Sciences (CAS) Graduate School, Chinese Academy of Sciences, Shenyang, China, in 2010.

He is currently a professor at the Shenyang Institute of Automation, Chinese Academy of Sciences, where he serves as director of the Intelligent Inspection and Equipment Research Laboratory.



Siyuan Wang (Student Member, IEEE) received his B.E. degree from Wuhan University of Technology in 2023.

Currently, he is a M.E. student at Shenyang Institute of Automation, Chinese Academy of Sciences. His current research interests include video generation, human pose estimation, and deep learning.



Zhi Han (Member, IEEE) received the B.Sc., M.Sc., and Ph.D. degrees in applied mathematics from Xi'an Jiaotong University (XJTU), Xi'an, China, in 2005, 2007, and 2012, respectively, and the joint Ph.D. degree in statistics from the University of California, Los Angeles (UCLA), Los Angeles, California, in 2011.

He is currently a professor at the State Key Laboratory of Robotics, Shenyang Institute of Automation, Chinese Academy of Sciences (SIA, CAS). His research interests include image/video modeling,

low-rank matrix recovery, and deep neural networks.